Estimating Functional Brain Networks by Low-Rank Representation With Local Constraint

Zhigang Li, Weimin Zheng, Honghong Liu, Jingyu Liu, Chang Yan, Zhiqun Wang, Bin Hu, *Fellow, IEEE*, and Qunxi Dong

***Abstract*— The functional architecture undergoes alterations during the preclinical phase of Alzheimer's disease. Consequently, the primary research focus has shifted towards identifying Alzheimer's disease and its early stages by constructing a functional connectivity network based on resting-state fMRI data. Recent investigations show that as Alzheimer's Disease (AD) progresses, modular tissue and connections in the core brain areas of AD patients diminish. Sparse learning methods are powerful tools for understanding Functional Brain Networks (FBNs) with Regions of Interest (ROIs) and a connectivity matrix measuring functional coherence between them. However, these tools often focus exclusively on functional connectivity measures, neglecting the brain network's modularity. Modularity orchestrates dynamic activities within the FBN to execute intricate cognitive tasks. To provide a comprehensive delineation of the FBN, we propose a local similarity-constrained low-rank sparse representation (LSLRSR) method that encodes modularity information under a manifold-regularized network learning framework and further formulate it as a low-rank sparse graph learning problem, which can be solved by an efficient optimization algorithm. Specifically, for each modularity structure, the Schatten p-norm regularizer reduces the reconstruction error and provides a better approximation of the low-rank constraint. Furthermore, we adopt a manifold-regularized local similarity prior to infer the intricate relationship between subnetwork similarity and modularity, guiding the modeling of FBN. Additionally, the proximal average method approximates the joint solution's proximal map, and the resulting nonconvex optimization problems are solved using the alternating direction multiplier method (ADMM). Compared to state-of-the-art methods for constructing FBNs, our algorithm generates a more modular FBN. This lays the groundwork for further research into alterations in brain network modularity resulting from diseases.**

***Index Terms*— Functional brain network, modularity, low rank, manifold-regularized, subnetwork similarity, sparsity.**

Manuscript received 14 April 2023; revised 23 September 2023 and 27 November 2023; accepted 11 January 2024. Date of publication 18 January 2024; date of current version 8 February 2024. This work was supported in part by the National Natural Science Foundation of China under Grant 62376030, Grant 62227807, Grant 62302044, Grant 62272044, Grant 32241027, Grant 61632014, Grant 61627808, and Grant 81873892; in part by the Technology Innovation 2030-Brain Science and Brain-Like Research under Grant 2021ZD0200601 and Grant 2021ZD0201900; in part by the Beijing Institute of Technology Research Fund Program for Young Scholars; in part by the National Key Research and Development Program of China under Grant 2022YFC3500503 and Grant 2019YFA0706200; in part by the China Postdoctoral Science Foundation Funded Project under Grant 2022M720434; in part by the Natural Science Foundation of Beijing Municipality under Grant 7222320; in part by the Capital Health Research and Development of Special Fund under Grant 2022-2-6081; and in part by the Scientific Research Fund of Aerospace Center Hospital under Grant YN201901. *(Zhigang Li and Weimin Zheng are co-first authors.) (Corresponding authors: Zhiqun Wang; Bin Hu; Qunxi Dong.)*

This work involved human subjects or animals in its research. Approval of all ethical and experimental procedures and protocols was granted by the Medical Research Ethics Committee of Xuanwu Hospital, and performed in line with the Declaration of Helsinki.

Zhigang Li, Honghong Liu, Jingyu Liu, Chang Yan, Bin Hu, and Qunxi Dong are with the School of Medical Technology, Beijing Institute of Technology, Beijing 100081, China (e-mail: lzg2021@bit.edu.cn; lhh2020@bit.edu.cn; liujingyu@bit.edu.cn; ychang0212@bit.edu.cn; bh@bit.edu.cn; dongqx@bit.edu.cn).

Weimin Zheng and Zhiqun Wang are with the Department of Radiology, Aerospace Center Hospital, Beijing 100049, China (e-mail: 1013135963@qq.com; wangzhiqun@126.com).

Digital Object Identifier 10.1109/TNSRE.2024.3355769

I. Introduction

ALZHEIMER'S disease (AD) is an irreversible neurodegenerative disorder, affecting approximately 47 million people worldwide, with expectations of the number tripling by 2050 [1], [2], [3]. Alzheimer's disease is related to changes in structural and functional connectivity within the brain regions [4], [5]. One approach to quantify complex brain interactions is to view the brain as a network of subnetworks or modules, namely Functional Brain Networks (FBNs). FBNs constructed from high-dimensional functional magnetic resonance imaging (fMRI) plays a crucial role in AD detection [4], [5], [6], [7]. Constructing a high-quality Functional Brain Network (FBN) is challenging due to limited understanding of the human brain and the presence of significant noise in observed data.

Despite these challenges, many FBN estimation methods have been developed in recent years [8], [9], [10]. The Pearson correlation (PC) coefficient [11], [12] is widely used to measure the correlation between brain regions. However, the PC only models the full correlations without excluding confounding effects from other brain regions, resulting in a large number of misconnections in the FBN [13], [14], [15]. In contrast, partial correlation methods [16], [17] address the perturbation of noise by regressing the confounding effects of other brain regions, and the resulting connections may be

ill-posed due to the curse of dimensionality. To solve this problem, the regularization term is typically introduced to stabilize the statistical estimation when building the FBN [18], [19], [20], and a method of incorporating a priori information into the graph learning framework is provided [21], [22]. For instance, Huang et al. [23] estimated FBN by constructing a sparse graph using a Gaussian graph model with l1 regularization, also known as a graphical lasso (GL). Ryali et al. [24] developed the sparse partial correlations elastic net penalty (SPC-EN), which combines $l1$ and $l2$ norms to determine the connections between brain regions. Yu et al. [25] proposed the strength-weighted sparse group representation (WSGR) method in which subnetworks with similar connections share regularization weights. This method cannot differentiate easily between the patient and control groups. To solve this problem, Yu et al. [26] used temporal correlation and intersubject correlation as a priori knowledge to guide group sparse representation (GSR)-based network modeling.

Existing FBN estimation methods typically focus solely on node similarity, neglecting the brain's modular organization [27], [28]. It is noteworthy that in recent work, Varoquaux et al. [29] described an FBN by identifying its modular structure in a decomposable graphical model. However, the modular structure identified by the greedy algorithm depends on the initial graph and is prone to local optimization. To solve this problem, Qiao et al. [30] formulated FBN estimation as a sparse low-rank graph learning problem. However, this method ignores the complex relationship between subnetwork similarity and modular structure. Research has shown that there is a close relationship between subnetwork similarity and modularity in brain networks [31], [32]. Specifically, regions within the same module show higher subnetwork similarity, while those in different modules show lower similarity levels.

Studies show that incorporating standardized prior biological and physiological knowledge of the brain [33] enhances FBN modeling. We guided modular FBN modeling through prior subnetwork similarity and completed FBN coding under the manifold-regularized framework. The proximal average method simplifies the algorithm, offering valuable insights into the brain's structure, organization, and implications for understanding function and pathology. The main contributions of this study are threefold:

(1) More modular FBNs were generated by combining the manifold regularization learning method and introducing the similarity prior of sub networks for structuring networks.

(2) Local popular regularization constraints enable the model to better capture local patterns and features in the data, reduce the sensitivity of the model to noisy data, and make the model more robust and stable.

(3)We have developed a learning framework based on LSLRSR for the use of RS-fMRI data for automatic brain disease identification. Finally, we validate our method using different RS-fMRI datasets.

The rest of this paper is organized as follows. In Section II, we introduce the related work. In Section III, we first introduce material and data preprocessing methods. Then, our proposed method and optimization model are introduced. In Section IV, we describe the experimental setup and evaluate our proposed method through AD recognition experiments. At the end of this section, we also discuss our findings and work prospects. In Section V, we summarize the paper.

II. Related Work

A. Matrix-Regularized Network Learning Framework

Studies show that the trade-off between fitting data efficiently and encoding biological or physical prior knowledge can be formulated using a regularized framework, extensively studied in statistics and machine learning [24], [34], [35]. Based on previous studies, Qiao et al. [30] formulated a matrix-regularized network learning framework as follows:

$$\min_{Z} f(\mathbf{X}, Z) + \lambda R(Z) \text{ s.t. } Z \in \Delta_* \tag{1}$$

where $X = [x_1, x_2, \cdots, x_n] \in R^{m \times n}$ is the mean time series of the ith subject, n is the number of ROIs in each subjects, the matrix Z encodes the strength of connections between different brain regions or ROIs. The regularization term $\lambda R(Z)$ is designed to incorporate prior knowledge about the brain's functional or structural properties. This regularization can encourage specific patterns of connectivity or sparsity in the network, which might be informed by biological or physical insights. Δ is a set of additional constraints on the network. FBN has modules in the network in which the nodes are densely connected within groups and in which the connections between these groups are sparse. Therefore, Qiao et al. [30] proposed a regularization framework based on modular prior knowledge, defined as follows:

$$\min_{Z_i} \|\mathbf{X} - \mathbf{X}Z\|_F^2 + \lambda \|Z\|_1 + \beta \|Z\|_* \tag{2}$$

where λ and β are regularization balance parameters, $\|\mathbf{X}-\mathbf{X}Z\|_F^2$ is the data-fitting term, $\|Z\|_1$ measures the sparsity of the network, and $\|Z\|_*$ represents modular modeling with Mate $\|Z\|_1$.

III. Material and Method

The pipeline of the proposed LSLRSR framework (see Fig. 1) is as follows: (1) First, the Data Processing Assistant for Resting-State fMRI (DPARSF) is applied to preprocess raw fMRI data and extract the signals of the brain region of interest (ROIs) according to the AAL template [36]; (2) Second, the FBN is constructed by the proposed LSLRSR method. (3) Last, the most discriminative features are selected by t test, and SVM is used for final classification.

A total of 219 right-handed subjects participated in the study, including 67 AD patients, 64 MCI (Mild Cognitive Impairment (MCI) is a transitional stage between normal age-related cognitive decline and more serious conditions such as dementia. Individuals with MCI may experience noticeable cognitive changes but generally maintain their ability to perform daily activities.) patients and 88 HCs. The protocol was approved by the Medical Research Ethics Committee and consent was obtained in accordance with the Declaration of Helsinki.

All participants underwent a complete physical and neuropsychological assessment, including the mini-mental state

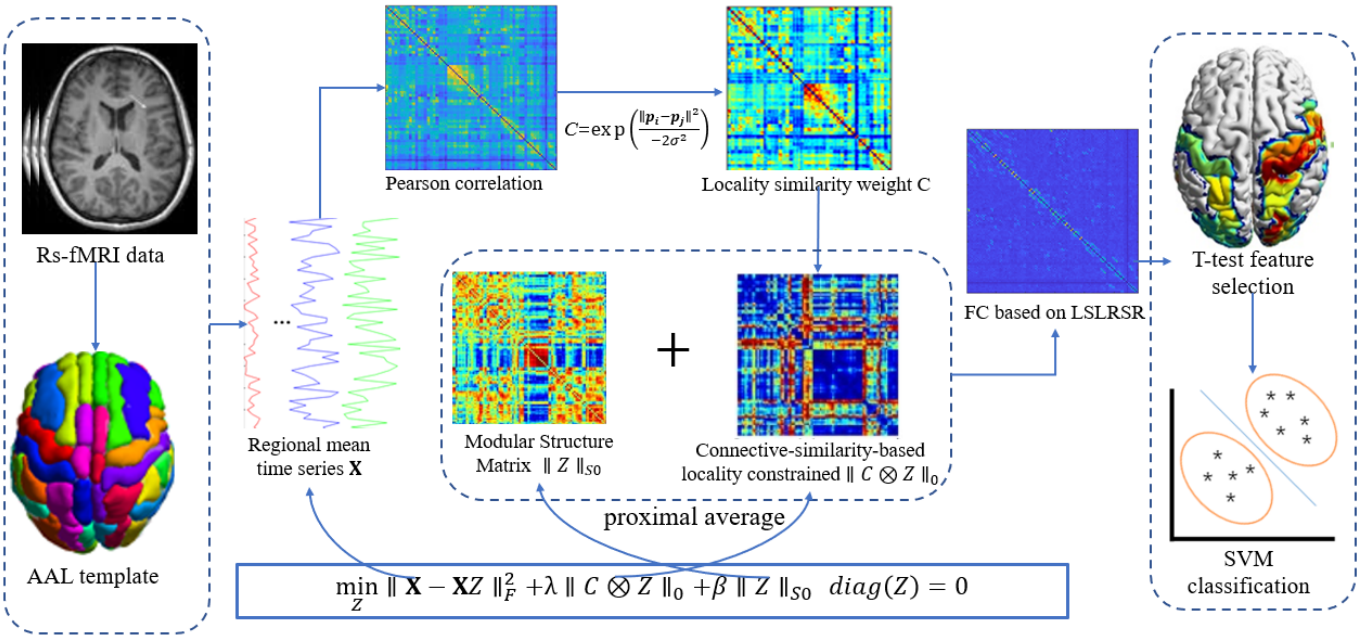

Fig. 1. Illustration of the proposed LSLRSR method.

examination (MMSE) and clinical dementia rating (CDR). The AD and MCI patients met the new research criteria for possible or probable AD and MCI, respectively [37].

The controls met the following criteria: (a) no visual loss or hearing loss, as well as other neurological deficiencies; (b) no stroke, depression or epilepsy, and no other neurological or psychiatric disorders; (c) no abnormal findings on routine brain MRI; (d) no cognition or memory complaints; and (e) a CDR score of 0.

A. fMRI Acquisition

he resting-state fMRI data were acquired axially using echo-planar imaging (EPI) with the following parameters: repetition time (TR) / echo time (TE) / flip angle (FA) / field of view (FOV)= 2000 ms/40 ms/90°/24 cm, image matrix = 64 × 64, slice number = 33, thickness = 3 mm, gap = 1 mm, band width = 2232 Hz/ pixel.

B. Data Preprocessing

fMRI data processing was performed using DPARSF (http//rfmri.org/DPARSF) [36]. The procedure included the following: (1) The first 10 volumes were removed. (2) Slice timing and head motion correction was performed; subjects with maximum head movements $>$ 2 mm in translation or $>$ 2° in rotation were excluded; (3) The realigned volumes were spatially normalized in the MNI space using the T1 template, and the functional images were resampled into a voxel size of $3\times3\times3$ mm^3; (4) The data were smoothed with a Gaussian filter of 4-mm FWHM to reduce noise and residual differences in gyral anatomy; (5) Regressing out the Friston-24 parameters, their first time-derivatives, and global, WM, and CSF signals; (6) Time band-pass filtering (0.01 – 0.08 Hz) was performed to reduce the effects of low-frequency drift and highfrequency physiological noise.

C. Proposed Method

The community structure of brain networks is portrayed as a hierarchy of modules, each comprising densely connected regional nodes. The similarity between brain subnetworks supports the modular structure, implying similar regions or modules may exist across individuals. However, current FBN modeling methods often overlook this inter-subnetwork similarity.

Exploring the link between subnetwork similarity and modularity enhances our understanding of brain function, cognitive processes, and disease progression. In many cases, a subnetwork is seen as a distinct structure within the network. When a subnetwork shares similarities with others, it forms an autonomous module. Quantifying subnetwork similarity involves measuring and transforming the distance between them into a similarity score. Incorporating prior knowledge provides effective guidance for modeling FBNs.

$$P_{ij}^{(PC)} = \frac{(x_i - \bar{x}_i)^T (x_j - \bar{x}_j)}{\sqrt{(x_i - \bar{x}_i)^T (x_i - \bar{x}_i)}\sqrt{(x_j - \bar{x}_j)^T (x_j - \bar{x}_j)}} \quad (3)$$

where $P_{ij}^{(PC)} \in P^{(PC)}$ represents the Pearson correlation between two-time series x_i and x_j refer to the time series data from two distinct brain regions. $P^{(PC)} = [p_1, p_2, \cdots, p_l] \in R^{n\times n}$ is the FBN based on Pearson correlation. i and $j = (1, 2, \cdots, n)$ indicate the respective nodes in a brain network.

$$C = \exp\left(\frac{\| p_i - p_j \|^2}{-2\sigma^2}\right) \quad (4)$$

where p_i and $p_j \in P^{(PC)}$ is the i-th and j-th column in $P^{(PC)}$ that represent the correlation vectors between the corresponding ROI and all other ROIs, C represents a measure of similarity or connection strength between p_i and p_j, in the functional brain network(FBN) $P_{ij}^{(PC)}$.

Previous research has shown a strong correlation between the similarity of subnetworks and their modularity [38], [39]. Taking inspiration from recent developments in manifold learning, we have integrated a locality-constrained factor into our approach, which explicitly considers the similarity among subnetworks within functional brain networks (FBNs). The majority of manifold learning algorithms [40], [41] employ the concept of local invariance. In essence, if two subnetworks share similar topological features, a significant weight is assigned between these two subnetworks. Following the approach outlined in [42], we utilize the following local constraints to reveal the similarity among subnetworks:

$$\|C \otimes Z\|_0 \tag{5}$$

where $\otimes$ denotes the Hadamard product, and the C local similarity constraint.

Existing studies describe modularity by combining low-rank with sparse representation. Modularity imposes stronger constraints on network structure compared to sparsity, as modularity implies sparsity. Integrating brain sparsity and modularity priors aids in estimating more reasonable brain networks. The similarity between brain modules reflects the brain's separation and integration, while the similarity of sub-networks within modules indicates module density. Introducing similarity priors to the brain network helps represent the brain more realistically. Combining formulas (2) and (5), we can express the FBN estimation model as:

$$\min_{Z_i} \|\mathbf{X} - \mathbf{X}Z\|_F^2 + \lambda\|C \otimes Z\|_0 + \beta\|Z\|_* \tag{6}$$

where $\|0\|_0$ is L0-norm, and $\|\cdot\|_*$ is trace norm. However, because the kernel norm is used to approximate the optimization model without considering the suppression of the extremely large singular values of the reconstructed data, there can be outliers in the eigenvalues. The Schatten-p [43], [44] norm can suppress singular values to a smaller range and is more able to approximate the rank. Thus, (6) becomes:

$$\min_{Z} \|\mathbf{X} - \mathbf{X}Z\|_F^2 + \lambda\|C \otimes Z\|_0 + \beta\|Z\|_{S0}\,\mathrm{diag}(Z) = 0 \tag{7}$$

where $\mathrm{diag}(Z) = 0$ is the constraint that is used to avoid the trivial solution of representing a data point as a linear combination of itself, and $\|*\|_{S0}$ is the Schatten-0 norm. The Schatten-0 norm exhibits more robustness to noise and outliers and can better learn similarities between data [45], [46].

D. Optimization Algorithm

To solve Z, we need to introduce a new variable to decompose the original problem into solving two variables J and Z. This leads us to solve the following equation:

$$\begin{aligned} &\min_{J,Z} \frac{1}{2}\|\mathbf{X} - JZ\|_F^2 + \lambda\|C \otimes Z\|_0 + \beta\|Z\|_{S0} \\ &\text{s.t. } J = Z - \mathrm{diag(Z)} \end{aligned} \tag{8}$$

the augmented lagrangian function of (8) is:

$$\begin{aligned} \mathcal{L}_\mu(J, Z, \Lambda) = &\frac{1}{2}\|\mathbf{X} - \mathbf{X}J\|_F^2 + \lambda\|C \otimes Z\|_0 + \beta\|Z\|_{S0} \\ &+ \frac{\mu}{2}\|J - Z + \mathrm{diag}(Z)\|_F^2 \\ &+ \langle\Lambda, J - Z + \mathrm{diag}(Z)\rangle \end{aligned} \tag{9}$$

where μ is the penalty parameter and Λ is the Lagrange multiplier. After that, we calculate the unknown variables by fixing the remaining variables.

Step 1. Update J^{k+1}, Assuming that variable Z^{k+1}, μ^{k+1}, Λ^{k+1} is known, variable J can be solved by minimizing the following problem:

$$J^{k+1} = \left[\mathbf{X}^{\mathrm{T}}\mathbf{X} + \mu^k\right]^{-1}\left[\mathbf{X}^{\mathrm{T}}\mathbf{X} + \mu^k Z^k - \Lambda^k\right] \tag{10}$$

Step 2. Update Z^{k+1}, assuming that variable J^{k+1}, μ^{k+1}, and Λ^{k+1} is known, the following problem can be solved:

$$\min_{z_i} \lambda\|C \otimes Z\|_0 + \beta\|Z\|_{S0} + \frac{\mu^k}{2}\left\|J^{k+1} + \frac{\Lambda^k}{\mu^k} - Z\right\|_F^2 \tag{11}$$

when $\lambda = 0$ the (11) can be expressed:

$$P_g^\mu = \min_{Z_i} \beta\|Z\|_{S0} + \frac{\mu^k}{2}\left\|J^{k+1} + \frac{\Lambda^k}{\mu^k} - Z\right\|_F^2 \tag{12}$$

where P_g^μ is the proximal operator of $\|Z\|_{S0}$. Let $U\Sigma V^T$ denote the SVD of $\left(J^{k+1} + \frac{\Lambda^k}{\mu^k}\right)$. So the solution of (11) can be expressed:

$$\boldsymbol{Z}^{k+1} = \boldsymbol{U}\boldsymbol{H}\left(\boldsymbol{\Sigma}; \frac{\beta}{\mu^k}\right)V^T \tag{13}$$

when $\beta = 0$ proximal map can be expressed:

$$P_f^\mu = \min_{Z} \lambda\|C \otimes Z\|_0 + \frac{\mu^k}{2}\left\|J^{k+1} + \frac{\Lambda^k}{\mu^k} - Z\right\|_F^2 \tag{14}$$

where P_g^μ is the proximal operator of $\|C \otimes Z\|_0$, the hard thresholding operator H applied entry-wise to matrix $\left(J^{k+1} + \frac{\Lambda^k}{\mu^k}\right)$. Introducing proximal averaging [47] in recent work allows us to efficiently solve the problem in (11) when $\lambda \neq 0$ and $\beta \neq 0$ resolved proximal map by averaging low-rank and sparse regularizer for proximal mapping $P_{i_{f+g}}^\mu$:

$$P_{f+g}^\mu \approx \lambda P_f^\mu + \beta P_g^\mu \tag{15}$$

where $\lambda + \beta = 1$.

Step3: Update Lagrange Multiplier Λ^{k+1} and μ^{k+1}. Assuming that variable J^{k+1}, Z^{k+1}, and μ^k are known, the following problem can be solved:

$$\Lambda^{k+1} = \Lambda^k + \mu^k\left(J^{k+1} - Z^{k+1}\right) \tag{16}$$

$$\mu^{k+1} = \min\left(\rho\mu^k, \mu^{\max}\right) \tag{17}$$

when the difference of J in two adjacent iterations is less than the predefined threshold, the iteration process is terminated, and $\rho > 1$ is the step size for adaptive changes in μ.

E. Constructing Low Rank Non-Negative Sparse Graphs

Given a BOLD signal matrix X through Section 2.3, we can optimize the coefficient matrix Z_i^*. The sparse constraint ensures that each region of interest is associated with only a few brain regions, so the graph from Z_i^* is naturally sparse. The low-rank time constraint can ensure that the coefficients of samples from the same subspace are highly correlated and fall into the same cluster, so Z_i^* can capture the global correlation

Algorithm 1 Locally Constrained Low-Rank Sparse Representation by ADMM Optimization

Input: ROI mean time series X, $\{\lambda, \beta\} > 0, \lambda + \beta = 1$
Output: low rank non-negative sparse graphs
1: Initialize: $\{J, Z, \Lambda\} = 0, \mu^{(0)} > 0$
2: Compute $\mathbf{X}^{\mathrm{T}}\mathbf{X}$
3: while not converged do
4: Update J^{k+1} by (10)
5: Normalize columns of J to unit to l2-norm
6: Calculate rank regularized proximal map P_g^{μ} by (12)
7: Calcultte sparsity regularized proximal map P_f^{μ} by(14)
8: Update $Z^{k+1} = P_{f+g}^{\mu}$ defined in (15,12,14)
9: Update Λ^{k+1} by (16)
10: Update μ^{k+1} by (17)
11: end while
12: Calculate graph weight matrix W by (18),(19),(20)

(i.e., cluster) of all the data. In fact, due to data noise, the Z_i^* is usually dense and small. So we can normalize the Z_i^* and set a threshold to control its sparsity:

$$Z_i^* = Z_i^* / \left\| Z_i^* \right\|_2 | \tag{18}$$

$$\widehat{Z_l^*} = \begin{cases} 0 & \text{if } Z_i^* < 0 \\ Z_i^* & \text{if } Z_i^* > 0 \end{cases} \tag{19}$$

after (19) we can obtain $\widehat{Z_l^*}$. Then we can define the graph weight matrix W as:

$$\mathrm{W} = \frac{\widehat{Z_l^*} + \left(\widehat{Z_l^*}\right)^T}{2} \tag{20}$$

The main steps of the proposed algorithm are summarized in Algorithm 1.

F. Feature Selection and Classification

We employ the simplest feature selection method (t test, p value = 0.05) and the most popular support vector machine (SVM) [48] classifier (in our linear kernel with default parameter C = 1) in the experiment.

Due to the limited data available, the FBN estimation methods involved were tested using a ten-fold cross-validation approach. Specifically, all samples are divided into ten parts, leaving only one part for testing, while the remaining parts are used for selecting features and training classifiers. Finally, the classification performance of different methods is evaluated by a set of commonly used quantitative metrics, including accuracy (Acc), sensitivity (Sen) and specificity (Spe). Additionally, the area under the ROC curve (AUC) is also adopted to measure the MCI and AD classification performance [49].

IV. Result

A. Dataset

To validate the generative performance of the proposed method, LSLRSR is applied to AD diagnosis and eyes open/close cognition tasks.

There were 219 participants, including 67 patients with AD (36 males), 64 MCI patients (24 males), and 88 (39 males) in the normal control group. Demographic characteristics are detailed in the paper [50].

To further verify the robustness of our algorithm, we conducted classification experiments on another dataset. The eyes open/close dataset was downloaded from the public dataset "Beijing Eyes Open Eyes Closed Study". fMRI data were recorded during eyes open (EO) and eyes closed (EC) states [51].

B. Experiments Set

In this paper, we verify the robustness of our algorithm through two different sets of experiments. (1) In the first set of experiments, we use the AD dataset to compare the results of different algorithms. We identify the optimal parameters by comparing all parameters in the algorithm using a linear search in the following range: [0.01, 0.025, 0.05, 0.075, 0.10, 0.25, 0.50, 0.75, 0.99]. (2) In the second set of experiments, we use the dataset provided by [51], and the parameter settings in the comparison algorithm are consistent with [51].

We used different methods to estimate the FBN based on the real AD dataset and the brain state dataset provided in the BrainNetClass tool [51]. We will briefly introduce the six methods below:

- Pearson's Correlation (PC) [51]: Network Construction using Pearson's Correlation of regional mean BOLD signals.
- Sparse Representation (SR) [51]: network construction using sparse representation.
- Weighted Sparse Representation (WSR) [25]: The original connection strength and its group structure are optimized by the connection strength weighted sparse group constraint to construct the functional connection network.
- Weighted Sparse Group Representation (WSGR) [52]: The constraint based on group structure is introduced to integrate link strength and group structure information to build the functional connection network.
- Strength and similarity guided GSR (SSGSR) [26]: This method employs integration of single functional connectivity (FC) information and introduces GSR-based network construction framework.
- Sparse Low-rank Representation (SLR) [30]: This method employs FC network construction using estimation schemes by encoding prior modularity in the form of matrix regularizer.
- Functional Brain Network Estimation with Human-Guided Modularity Representation (FBNMR) [32]:FC network construction is performed using an estimation scheme by encoding both prior modular topology and expert domain knowledge.
- Functional Brain Network Estimation With Time Series Self-Scrubbing (FBNSS) [31]: The method employs FC network construction using an estimation scheme by introducing a latent variable as an indicator of the data quality.

Thus, we set parameter λ by a linear search in the range of [0.01, 0.025, 0.05, 0.075, 0.10, 0.25, 0.50, 0.75, 0.99]. We performed a validation analysis of the method. After obtaining the FC of all participants, we used them to identify MCI and AD from the NC.

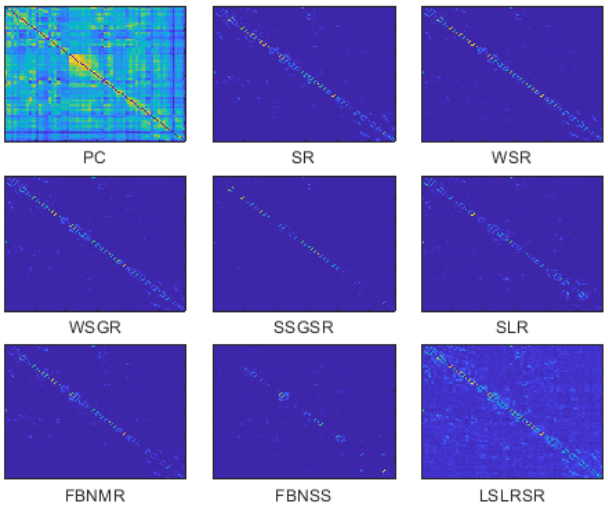

Fig. 2. The adjacency matrices of the estimated FC by PC, SR, WSR, WSGR, SSGSR, SLR, FBNMR, FBNSS and LSLRSR. Note that all weights are normalized to the interval -1 to 1 for convenience of comparison between different methods. for convenience of comparison between different methods.

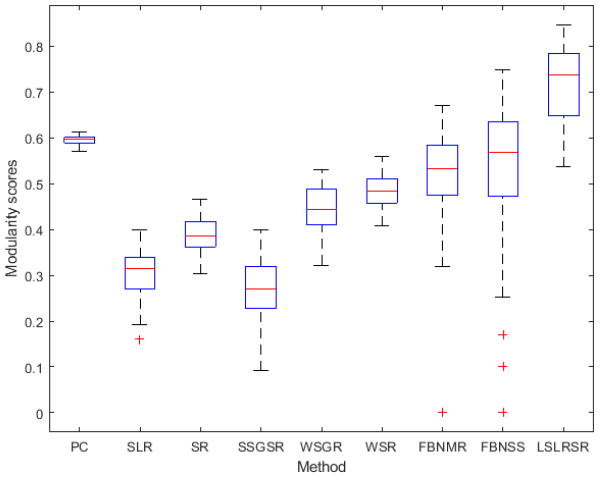

Fig. 3. Modularity scores of networks constructed by different methods. The red line within each box represents the sample median. The upper and lower edges of each box represent the upper and lower quartiles, respectively. The "+" is outliers.

C. FBN Estimation

The representative FBNs of NCs as estimated by eight different methods are presented in Fig. 2. For the convenience of observation, all weights are normalized into the interval $[-1\ 1]$. This figure demonstrates that the FBNs based on PC and the other methods have different topological structures, and the FBNs based on SR, WSR, WSGR, SSGSR, SLR, FBNMR, FBNSS and LSLRSR have similar topological properties. The reason why PC and other algorithms have different topologies is that they use different data fitting functions. SLR and our proposed method (LSLRSR) share similar topological properties. Among these methods, SLR, FBNMR, FBNSS and other methods show a clear modular structure. Unlike SLR, FBNMR and FBNSS, our algorithm shows a tighter internal modular structure due to the introduction of local similarity functions. ground connection. Unlike from SLR, LSLRSR-based methods preserve sub-network features with similar topological properties due to local similarity prior knowledge.

In addition, to quantitatively evaluate modularity, we used Newman's spectral algorithm [53] to calculate the modularity scores Q of different constructed brain networks.

$$Q = 1/(2m)\sum_{ij}\left(Z_{ij} - k_i k_j/(2m)\right)\delta\left(L_i, L_j\right) \tag{21}$$

where m is the total number of edges in the network, Z is the adjacency matrix corresponding to the network, $Z_{ij} = 1$ means that there is an edge between node i and node j, and k_i is the degree of node i, and L_i is the label that node i belongs to a certain community.

It is worth noting that negative edge weights are invalid for the Newman algorithm, and we deleted all edge weights less than 0 [30], [53]. In addition, all parameters in this experiment are the optimal parameters in the training process (that is, the classification accuracy is the highest). Fig. 3. presents the boxplots of the modularity scores for several different methods. As shown in the figure, our method retains the most modular structure under the optimal parameters (when the classification accuracy is the highest) compared with several other methods. At the same time, there are significant differences between the highest and lowest modularity scores of different nodes. Due to the use of the S0 norm as a constraint, our algorithm reduces the occurrence of outliers relative to SLR.

In the data, our method outperforms several alternatives, maintaining a prominent modular structure, especially under optimal parameters when classification accuracy is at its peak. Notably, there is a significant contrast in modularity scores among different nodes. Incorporating the S0 norm as a constraint helps our algorithm reduce outliers compared to the SLR approach.

The PC-based method, being fully connected, exhibits a higher modular structure than other methods (excluding ours). Unlike conventional approaches, our algorithm achieves a richer abundance of FBN modular structures. This success is attributed to the integration of local similarity constraints, guiding the modeling of the functional connectivity network. This results in enhanced cohesion within each module's connections, while interconnections between distinct modules become more sparse.

D. Classification Results

For each method employed in network modeling, feature vectors are constructed by connecting the upper triangular elements of each subject's network representation. To clarify, the dimensionality of these feature vectors is determined as follows. Subsequently, we apply two-sample t-tests with a significance level of $p < 0.05$ (uncorrected) during the feature selection process in order to reduce redundancy. Table II and Figure 4 present the classification performance of various methods for queues related to Alzheimer's Disease (AD) and queues associated with (EO/EC). We employed Z-scores to compute the variances between distinct algorithms, and the outcomes are displayed in Table I.

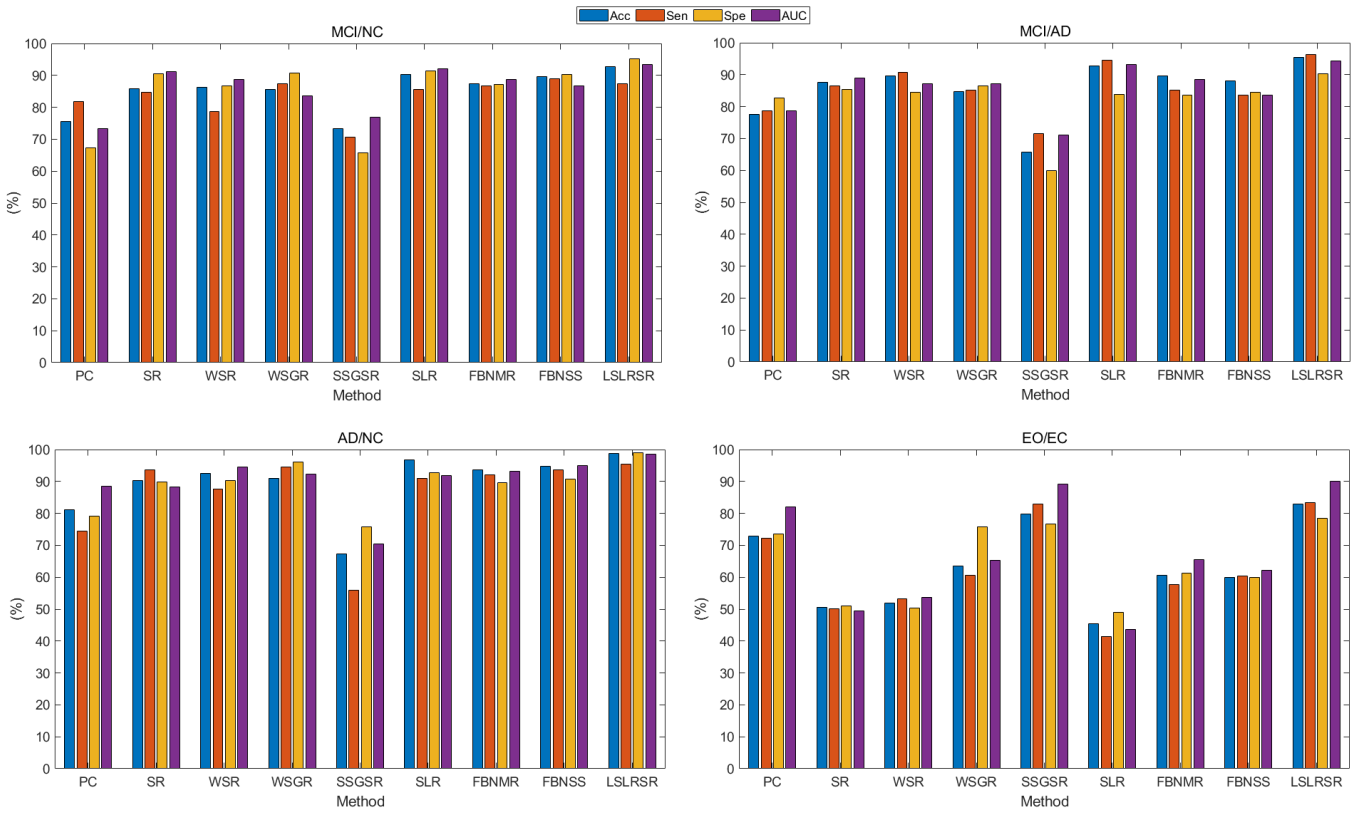

Fig. 4. Results (%) of nine different methods in MCI vs. NC, MCI vs. AD, AD vs. NC, EO vs. EC classification.

TABLE I
RESULTS SHOW SIGNIFICANT DIFFERENCES BETWEEN EIGHT DIFFERENT METHODS AND LSLRSR ACROSS VARIOUS CLASSIFICATION TASKS

Method	PC	SR	WSR	WSGR	SSGSR	SLR	FBNMR	FBNSS
MCI/NC	< 0.05	0.03	0.04	0.03	< 0.05	0.25	0.07	0.19
MCI/AD	< 0.05	0.02	0.05	< 0.05	< 0.05	0.21	0.05	0.02
AD/NC	< 0.05	< 0.05	< 0.05	< 0.05	< 0.05	< 0.05	< 0.05	< 0.05
EO/EC	< 0.05	< 0.05	< 0.05	< 0.05	0.24	< 0.05	< 0.05	< 0.05
AD/MCI/NC	< 0.05	< 0.05	< 0.05	< 0.05	< 0.05	< 0.05	< 0.05	< 0.05

TABLE II
RESULTS (%) OF NINE DIFFERENT METHODS IN AD VS. MCI VS. NC CLASSIFICATION

Method	Acc (%)	Sen (%)	Spe (%)
PC	37.73	37.10	68.62
SR	36.99	36.74	68.24
WSR	51.60	53.91	76.57
WSGR	49.09	50.13	74.52
SSGSR	51.14	46.62	73.52
SLR	50.68	49.92	74.82
FBNMR	67.69	65.81	70.65
FBNSS	66.59	68.92	67.35
LSLRSR	**84.19**	**79.16**	**83.21**

The proposed method, LSLRSR, outperforms other modeling methods across all performance indicators. Specifically, in MCI/NC classification, LSLRSR achieves an improvement of approximately 17% (up to 92.70%) compared to Pearson's modeling method, a 2% improvement compared to SLR, and approximately 7% improvement compared to other sparse representation-based modeling methods. Significance tests (p-values) indicate that PC, SR, WSR, WSGR, and SSGSR exhibit significant performance differences ($p < 0.05$), while SLR, FBNMR, and FBNSS show no significant difference ($p > 0.05$).

In MCI/AD classification, LSLRSR maintains significant advantages compared to other methods, with an 18% improvement over PC, 3% over SLR, and 6% over sparse representation methods. Sensitivity (96.37%) is significantly higher than specificity (90.23%). Significant performance differences ($p < 0.05$) are observed for PC, SR, WSR, and SSGSR, while SLR and FBNMR suggest possible differences ($p = 0.21$ and 0.05, respectively), and FBNSS exhibits a significant difference ($p = 0.02$).

In AD/NC classification, LSLRSR achieves an accuracy of 98.71%, an 18% improvement over the PC method and approximately 6% over sparse representation methods. All methods, except SLR, show significant performance differences ($p < 0.05$), while SLR suggests a potential difference ($p = 0.01$).

For EO/EC classification (as shown in Fig. 4), LSLRSR achieves better performance, reaching 82.98%. Compared to other methods, it shows a 13% improvement over the PC-based method, 40% over SLR, and 35% over SR and WSR. WSGR shows a 22% improvement, and SSGR demonstrates a 6% improvement. Significance tests indicate potential differences for PC and SR ($p = 0.02$ and < 0.05, respectively), while WSR, WSGR, SSGSR, SLR, FBNMR, and FBNSS show significant differences ($p < 0.05$).

Across a myriad of classification endeavors and diverse datasets, our innovative algorithm has triumphantly secured its position at the helm of performance. Previous research underscores a noteworthy phenomenon: the intricate modular transformations that the functional brain network (FBN) of patients afflicted with Alzheimer's disease (AD) undergoes. Our findings cast light on an intriguing possibility—by introducing localized similarity constraints, we gain a more intricate representation of the cerebral landscape, thus cultivating a decidedly modular brain network. This advance simultaneously establishes a bedrock for unceasing exploration into the evolutionary trajectory of brain network modularization amidst the intricate tapestry of AD's pathological progression. Our proposed algorithm has demonstrated remarkable performance across various classification tasks and datasets. Previous research has highlighted a significant shift in the modular structure of patients' Functional Brain Networks (FBN) during the progression of Alzheimer's Disease (AD). We findings show that introducing the S0 norm leads to the creation of smoother modular brain networks, effectively reducing the occurrence of abnormal values in brain modularity. Simultaneously, the incorporation of local similarity constraints proves to be a valuable guide for modeling modular brain networks. This approach results in sparser connections between brain modules and denser connections within modules. Enhancing modularity within the brain network contributes to our deeper understanding of the brain. Furthermore, our classification results underscore the effectiveness of modular brain networks in enhancing our comprehension and recognition of diseases and various brain states. These outcomes also serve as a foundational stepping stone for future investigations into the evolving modularity of brain networks during the pathological progression of AD.

E. Parameter and Noise Sensitivity

In this experiment, we have two parameters, the balance parameter λ and β (controls the sparsity of functional connectivity). Since $\lambda + \beta = 1$ in our algorithm (see Section II for details), we can only look at the sensitivity of λ. To verify the effect of different parameters on the accuracy, we take the value of the parameter within a certain range to see the effect of different parameters on our experimental results. Fig. 7 presents the results of two different parameters.

Fig. 7 presents the effect of parameter λ on the accuracy of the two classification and triple classification experiments. It can be seen from the figure that when parameter λ is taken as 0.01 and 0.25, the accuracy of different classifications reaches the maximum. In the process of parameter λ change, the trend of accuracy change is not obvious.

To verify the sensitivity of our algorithm to noise, we conducted experiments on binary classification tasks. We added 10DB of Gaussian white noise to the BOLD signal and compared the accuracy of all algorithms.

The experimental results for the binary classification task are depicted in the figure. From these results, it is evident that (1) as the level of noise intensity rises, the accuracy of all algorithms decreases to varying degrees. It's apparent that the presence of feature noise in the samples significantly impacts the classifier's classification performance. (2) Based on Figure 5, it's apparent that the traditional PC-based functional connectivity method is particularly susceptible to noise, resulting in a notable accuracy decrease of 53.08%. Compared to methods based on SR, WSR, WSGR, SSGSR, SLR, FBNMR, and FBNSS, these methods are not sensitive to noise, so their classification accuracy is better than traditional methods. The proposed LSLRSR algorithm achieved the best classification performance. The LSLRSR algorithm introduces the lowest rank constraint of S0 norm, which weakens the "influence" of larger singular values in the objective function, and weakens the influence of Outlier in the data on the signal. In addition, combining local constraints of manifold learning enables the LSLRSR algorithm to mine the geometric structure of samples in low dimensional space through low rank learning, maximizing the preservation of the modular structure of the brain network. Therefore, the intra class similarity and inter class differences of the data are more prominent, which enables the LSLRSR algorithm to achieve good classification performance in the presence of noise.

F. Complexity Analysis

We now investigate the computational cost of the LSLRSR and report the running time of different methods in AD vs. NC classification in Table III. As can be observed from Table III, the overall running time of our method is reasonable and acceptable in practical applications. However, the proposed LSLRSR requires more running time than PC, SR, and WSR because of the time spent computing the local similarity of the brain network. In our future work, we will optimize the algorithm to reduce the time complexity.

G. Compared With State-of-the-Art Methods

In addition to the above experimental analysis, we also compare the performance of our proposed LSLRSR method with that of several recent state-of-the-art studies, which are also performed on AD diagnosis (see Table IV). A brief introduction to these latest technologies is as follows. Ma et al. [54] introduced the Riemannian manifold model to extract global features for the diagnosis of ADd. Hu et al. [55] proposed a multi-band fusion model to estimate brain networks. These constructed brain networks were then subjected to graph

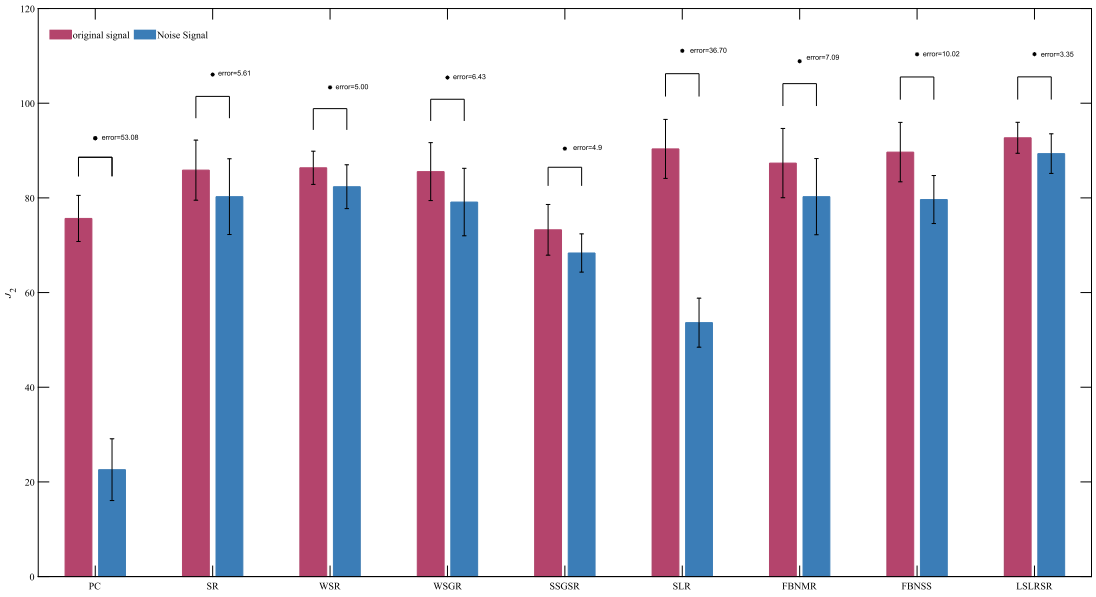

Fig. 5. Influence of noise on LSLRSR in classification tasks.

TABLE III
RESULTS (S) OF NINE DIFFERENT METHODS IN AD VS. MCI VS. NC CLASSIFICATION

Method	PC	SR	WSR	WSGR	SSGSR	SLR	FBNMR	FBNSS	LSLRSR
Times(s)	2.89	19.18	14.84	220.67	101.25	286.36	300.65	343.26	37.26

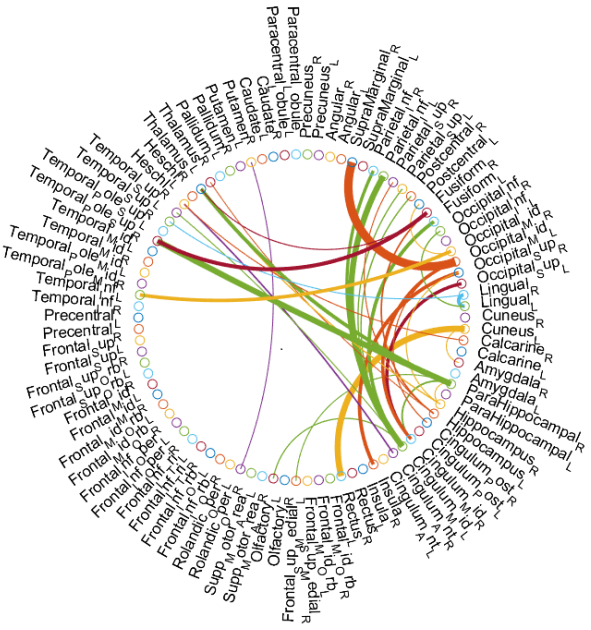

Fig. 6. The most discriminative features selected by the best accuracy of AD identification (i.e., AD vs. MCI vs. NC classification) and ASD identification tasks based on AAL template respectively. Note that, each arc shows the selected feature between two ROIs, where the color is randomly allocated only for a better visualization, and the thickness of each arc indicates its discriminative power that is inversely proportional to the corresponding the $p-value$.

theoretical analysis to differentiate MCI individuals from NC subjects. Wang et al. [56] proposed a distribution-guided network threshold learning (DNTL) method for FC network analysis to identify brain diseases through rs-fMRI. Zhang et al. [57] A multi-view feature learning method based on multi-map FC network to improve MCI diagnosis. Xue et al. [58] introduced a latent variable to control the volume sequence, thereby encoding the time dependence and sequential information of the signal into the estimated BFN. Zhang et al. [59] developed a multi-scale time series kernel-based learning model based on Jensen-Shannon divergence for brain disease diagnosis. Among all these compared methods, our method achieves the best classification performance with higher ACC, AUC, and SPE.

Table IV presents a comprehensive overview of the comparison conducted between our proposed methodology and six state-of-the-art (SOTA) approaches. The results of this comparative analysis indicate that our method attains the highest level of accuracy, reaching an impressive 98.18%, 95.42%, 92.70%, 84.19% in the classification of AD/NC,AD/MCI,MCI/NC and AD/MCI/NC. Furthermore, in contrast to various deep learning algorithms, our approach effectively identifies the specific brain regions and connections that are associated with diseases, rendering it more interpretable. Consequently, our method exhibits significant potential for facilitating clinical applications, particularly in the early detection of Alzheimer's disease-related brain functional connectivity dysfunction.

H. Discriminative Features

Using the optimal network parameters, as shown in Fig.6, we use the LSLRSR method to build a feature-connected

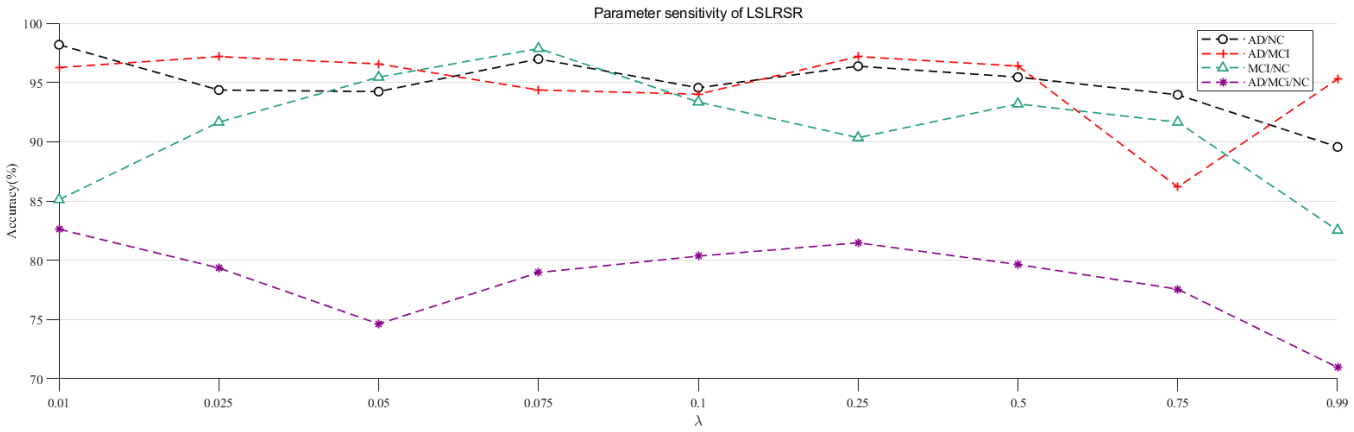

Fig. 7. Influence of λ and β on LSLRSR in four classification tasks, i.e., AD vs. MCI, AD vs. NC, and MCI vs. NC and AD vs. MCI vs. NC classification.

TABLE IV
RESULTS OF COMPARED WITH STATE-OF-THE-ART METHODS

Method	classification	AD/NC	AD/MCI	NC/MCI	AD/MCI/NC
Hu et.al. [55]	SVM	90.18	NA	NA	NA
Ma et. al. [54]	Softmax	92.87	87.29	85.13	83.78
Wang et. al. [56]	SVM	NA	NA	79.2	NA
Zhang et. al. [57]	SVM	NA	NA	85.5	NA
Xue et. al. [58]	SVM	NA	NA	90.51	NA
Zhang et. al. [59]	SVM	86.23	NA	NA	NA
Ours	**SVM**	**98.71**	**95.42**	**92.70**	**84.19**

network and use the t test method to rank all features. We choose the 34 significant frequently occurring values (p value < 0.05). The thickness of each arc in Figure 5 represents the discriminative power of the corresponding connection (rather than its actual connection strength). We found some of these biological links to AD recognition. Specifically, the middle temporal gyrus, hippocampus, parahippocampus, medial and accessory cingulate gyrus, thalamus, medial superior frontal gyrus, supramarginal gyrus, and inferior temporal gyrus have strong discriminative ability, which is consistent with similar pathological studies of MCI [60], [61], [62].

The default network is related to high-level cognitive functions such as self-awareness, memory, emotional processing, and psychological exploration [63]. Existing studies have found that changes in the default network connection pattern can be observed in AD and MCI [64]. A large number of studies have shown that the hippocampus in the early stage of AD is very sensitive to pathological onset [65], [66]. Alzheimer's patients may have abnormalities in memory, object recognition or information evaluation [67], because of the structure of the posterior cingulate gyrus., functional and metabolic abnormal changes [68], [69].

In addition to the DMN, there are other selected brain region connections shown to be important in AD diagnosis. Connectivity abnormalities have also been observed in the olfactory cortex of AD patients [70], and abnormal olfactory function has become a biomarker for AD and its early diagnosis [71]. At the same time, the inferior temporal gyrus is affected in AD patients [72], and its multimodal association area and high-level brain functions such as speech fluency will also undergo significant changes [73].

V. CONCLUSION

In this study, we propose a new FBN modeling method called LSLRSR, which utilizes prior similarity between sub-networks to guide functional brain network modeling and generate a more modular FBN. We introduce the Schatten-0 norm, which enhances the robustness of the FBN to the effects of signal noises and outliers and is better at capturing the modular structure in brain networks than sparse representation-based graphs. Experimental results demonstrate that the network constructed by our algorithm can retain more prior biological knowledge. Finally, we use the constructed feature connection network for MCI recognition, and even with a simple feature selection and classification pipeline, we can achieve an encouraging accuracy rate of 94.71% for MCI and 98.70% for AD, the three-category result reached 82%, meanwhile, the EO/ while the EO/EC result reached 82.98%

ACKNOWLEDGMENT

The authors would like to thank the study investigators and a patients who participated in the original trial.

REFERENCES

[1] C. A. Lane, J. Hardy, and J. M. Schott, "Alzheimer's disease," *Eur. J. Neurol.*, vol. 25, pp. 59–70, Jan. 2018. [Online]. Available: https://www.ncbi.nlm.nih.gov/pubmed/28872215

[2] A. Serrano-Pozo, M. P. Frosch, E. Masliah, and B. T. Hyman, "Neuropathological alterations in Alzheimer disease," *Cold Spring Harbor Perspect. Med.*, vol. 1, no. 1, Sep. 2011, Art. no. a006189. [Online]. Available: https://www.ncbi.nlm.nih.gov/pubmed/22229116

[3] E. Nichols et al., "Estimation of the global prevalence of dementia in 2019 and forecasted prevalence in 2050: An analysis for the global burden of disease study 2019," *Lancet Public Health*, vol. 7, no. 2, pp. 105–125, 2022.

[4] B. T. Thomas Yeo et al., "The organization of the human cerebral cortex estimated by intrinsic functional connectivity," *J. Neurophysiol.*, vol. 106, no. 3, pp. 1125–1165, Sep. 2011. [Online]. Available: https://www.ncbi.nlm.nih.gov/pubmed/21653723

[5] C. J. Honey et al., "Predicting human resting-state functional connectivity from structural connectivity," *Proc. Nat. Acad. Sci. USA*, vol. 106, no. 6, pp. 2035–2040, Feb. 2009. [Online]. Available: https://www.pnas.org/doi/abs/10.1073/pnas.0811168106

[6] O. Sporns, G. Tononi, and R. Kötter, "The human connectome: A structural description of the human brain," *PLoS Comput. Biol.*, vol. 1, no. 4, p. e42, 2005. [Online]. Available: https://www.ncbi.nlm.nih.gov/pubmed/16201007

[7] M. P. van den Heuvel and H. E. H. Pol, "Exploring the brain network: A review on resting-state fMRI functional connectivity," *Eur. Neuropsychopharmacology*, vol. 20, no. 8, pp. 519–534, Aug. 2010. [Online]. Available: https://www.ncbi.nlm.nih.gov/pubmed/20471808

[8] T. K. Khan, "An algorithm for preclinical diagnosis of Alzheimer's disease," *Frontiers Neurosci.*, vol. 12, p. 275, Apr. 2018.

[9] M. Tanveer et al., "Machine learning techniques for the diagnosis of Alzheimer's disease: A review," *ACM Trans. Multimedia Comput. Commun. Appl.*, vol. 16, no. 1s, pp. 1–35, Apr. 2020.

[10] M. B. T. Noor, N. Z. Zenia, M. S. Kaiser, S. A. Mamun, and M. Mahmud, "Application of deep learning in detecting neurological disorders from magnetic resonance images: A survey on the detection of disease and schizophrenia," *Brain Informat.*, vol. 7, no. 1, pp. 1–21, Dec. 2020.

[11] M. Song et al., "Brain spontaneous functional connectivity and intelligence," *NeuroImage*, vol. 41, no. 3, pp. 1168–1176, Jul. 2008.

[12] M. Rubinov and O. Sporns, "Complex network measures of brain connectivity: Uses and interpretations," *NeuroImage*, vol. 52, no. 3, pp. 1059–1069, Sep. 2010.

[13] Y. Osmanlioglu, J. A. Alappatt, D. Parker, and R. Verma, "Connectomic consistency: A systematic stability analysis of structural and functional connectivity," *J. Neural Eng.*, vol. 17, no. 4, Jul. 2020, Art. no. 045004.

[14] J. Wang et al., "Test-retest reliability of functional connectivity networks during naturalistic fMRI paradigms," *Hum. Brain Mapping*, vol. 38, no. 4, pp. 2226–2241, Apr. 2017.

[15] G. Deco and V. K. Jirsa, "Ongoing cortical activity at rest: Criticality, multistability, and ghost attractors," *J. Neurosci.*, vol. 32, no. 10, pp. 3366–3375, Mar. 2012.

[16] S. M. Smith et al., "Network modelling methods for FMRI," *NeuroImage*, vol. 54, no. 2, pp. 875–891, Jan. 2011.

[17] P. Fransson and G. Marrelec, "The precuneus/posterior cingulate cortex plays a pivotal role in the default mode network: Evidence from a partial correlation network analysis," *NeuroImage*, vol. 42, no. 3, pp. 1178–1184, Sep. 2008.

[18] Y. Du, X. Lin, M. Pham, and A. Ruszczynski, "Selective linearization for multi-block statistical learning," *Eur. J. Oper. Res.*, vol. 293, no. 1, pp. 219–228, Aug. 2021.

[19] L. Qiao, L. Zhang, S. Chen, and D. Shen, "Data-driven graph construction and graph learning: A review," *Neurocomputing*, vol. 312, pp. 336–351, Oct. 2018.

[20] S. Zhang, T. Zhang, X. Li, L. Guo, and T. Liu, "Joint representation of cortical folding, structural connectivity and functional networks," in *Proc. IEEE 15th Int. Symp. Biomed. Imag. (ISBI)*, Apr. 2018, pp. 1–5.

[21] C. C. Hilgetag, R. Kötter, K. E. Stephan, and O. Sporns, "Computational methods for the analysis of brain connectivity," in *Computational Neuroanatomy: Principles and Methods*. Springer, 2002, pp. 295–335.

[22] R. Kötter and K. E. Stephan, "Network participation indices: Characterizing component roles for information processing in neural networks," *Neural Netw.*, vol. 16, no. 9, pp. 1261–1275, Nov. 2003.

[23] S. Huang et al., "Learning brain connectivity of Alzheimer's disease by sparse inverse covariance estimation," *NeuroImage*, vol. 50, no. 3, pp. 935–949, Apr. 2010.

[24] S. Ryali, T. Chen, K. Supekar, and V. Menon, "Estimation of functional connectivity in fMRI data using stability selection-based sparse partial correlation with elastic net penalty," *NeuroImage*, vol. 59, no. 4, pp. 3852–3861, Feb. 2012.

[25] R. Yu, H. Zhang, L. An, X. Chen, Z. Wei, and D. Shen, "Connectivity strength-weighted sparse group representation-based brain network construction for MCI classification," *Human Brain Mapping*, vol. 38, no. 5, pp. 2370–2383, May 2017.

[26] Z. Yu, Z. Han, X. Chen, M. Liu, and D. Shen, "Strength and similarity guided group-level brain functional network construction for MCI diagnosis," *Pattern Recognit.*, vol. 88, pp. 421–430, Apr. 2018.

[27] M. Valencia, M. A. Pastor, M. A. Fernández-Seara, J. Artieda, J. Martinerie, and M. Chavez, "Complex modular structure of large-scale brain networks," *Chaos, Interdiscipl. J. Nonlinear Sci.*, vol. 19, no. 2, Jun. 2009, Art. no. 023119.

[28] K. Fang, B. Sivakumar, and F. M. Woldemeskel, "Complex networks, community structure, and catchment classification in a large-scale river basin," *J. Hydrol.*, vol. 545, pp. 478–493, Feb. 2017.

[29] G. Varoquaux, A. Gramfort, J. B. Poline, and B. Thirion, "Markov models for fMRI correlation structure: Is brain functional connectivity small world, or decomposable into networks?" *J. Physiol.-Paris*, vol. 106, nos. 5–6, pp. 212–221, Sep. 2012.

[30] L. Qiao, H. Zhang, M. Kim, S. Teng, L. Zhang, and D. Shen, "Estimating functional brain networks by incorporating a modularity prior," *NeuroImage*, vol. 141, pp. 399–407, Nov. 2016.

[31] F. Luo, Y. Yang, C.-F. Chen, R. Chang, J. Zhou, and R. H. Scheuermann, "Modular organization of protein interaction networks," *Bioinformatics*, vol. 23, no. 2, pp. 207–214, Jan. 2007.

[32] V. D. Blondel, J.-L. Guillaume, R. Lambiotte, and E. Lefebvre, "Fast unfolding of communities in large networks," *J. Stat. Mech., Theory Exp.*, vol. 2008, no. 10, Oct. 2008, Art. no. P10008.

[33] A. N. Khambhati, M. G. Mattar, N. F. Wymbs, S. T. Grafton, and D. S. Bassett, "Beyond modularity: Fine-scale mechanisms and rules for brain network reconfiguration," *NeuroImage*, vol. 166, pp. 385–399, Feb. 2018.

[34] Y. Zhang, G. Zhou, J. Jin, Q. Zhao, X. Wang, and A. Cichocki, "Sparse Bayesian classification of EEG for brain–computer interface," *IEEE Trans. Neural Netw. Learn. Syst.*, vol. 27, no. 11, pp. 2256–2267, Nov. 2016.

[35] P. M. Rasmussen, L. K. Hansen, K. H. Madsen, N. W. Churchill, and S. C. Strother, "Model sparsity and brain pattern interpretation of classification models in neuroimaging," *Pattern Recognit.*, vol. 45, no. 6, pp. 2085–2100, Jun. 2012.

[36] C. Yan and Y. Zang, "DPARSF: A MATLAB toolbox for 'pipeline' data analysis of resting-state fMRI," *Frontiers Syst. Neurosci.*, vol. 4, p. 1377, May 2010.

[37] Y. Stern et al., "Research criteria for the diagnosis of Alzheimer's disease: Revising the NINCDS-ADRDA criteria," *Lancet Neurol.*, vol. 6, no. 8, pp. 734–746, 2013.

[38] J. Du, L. Wang, B. Jie, and D. Zhang, "Network-based classification of ADHD patients using discriminative subnetwork selection and graph kernel PCA," *Computerized Med. Imag. Graph.*, vol. 52, pp. 82–88, Sep. 2016.

[39] K. R. A. Van Dijk, T. Hedden, A. Venkataraman, K. C. Evans, S. W. Lazar, and R. L. Buckner, "Intrinsic functional connectivity as a tool for human connectomics: Theory, properties, and optimization," *J. Neurophysiol.*, vol. 103, no. 1, pp. 297–321, Jan. 2010.

[40] J. Wang, J. Yang, K. Yu, F. Lv, T. Huang, and Y. Gong, "Locality-constrained linear coding for image classification," in *Proc. IEEE Comput. Soc. Conf. Comput. Vis. Pattern Recognit.*, Jun. 2010, pp. 3360–3367.

[41] J. Zheng, P. Yang, S. Chen, G. Shen, and W. Wang, "Iterative re-constrained group sparse face recognition with adaptive weights learning," *IEEE Trans. Image Process.*, vol. 26, no. 5, pp. 2408–2423, May 2017.

[42] L. Wei, A. Wu, and J. Yin, "Latent space robust subspace segmentation based on low-rank and locality constraints," *Exp. Syst. Appl.*, vol. 42, no. 19, pp. 6598–6608, Nov. 2015.

[43] Y. Xie, S. Gu, Y. Liu, W. Zuo, W. Zhang, and L. Zhang, "Weighted schatten p-norm minimization for image denoising and background subtraction," *IEEE Trans. Image Process.*, vol. 25, no. 10, pp. 4842–4857, Oct. 2016.

[44] J. Fan, L. Ding, Y. Chen, and M. Udell, "Factor group-sparse regularization for efficient low-rank matrix recovery," in *Proc. Adv. Neural Inf. Process. Syst.*, vol. 32, 2019, pp. 1–11.

[45] F. M. Paula, T. R. de Oliveira, and M. S. Sarandy, "Geometric quantum discord through the schatten 1-norm," *Phys. Rev. A, Gen. Phys.*, vol. 87, no. 6, p. 4996, Jun. 2013.

[46] M. Brbic and I. Kopriva, "ℓ_0-motivated low-rank sparse subspace clustering," *IEEE Trans. Cybern.*, vol. 50, no. 4, pp. 1711–1725, Apr. 2020.

[47] Y.-L. Yu, "Better approximation and faster algorithm using the proximal average," in *Proc. Adv. Neural Inf. Process. Syst.*, vol. 26, 2013, pp. 1–9.

[48] C.-C. Chang and C.-J. Lin, "LIBSVM: A library for support vector machines," *ACM Trans. Intell. Syst. Technol.*, vol. 2, no. 3, pp. 1–27, Apr. 2011.

[49] J. A. Hanley and B. J. McNeil, "The meaning and use of the area under a receiver operating characteristic (ROC) curve," *Radiology*, vol. 143, no. 1, pp. 29–36, 1982.

[50] W. Zheng et al., "Application of generalized split linearized Bregman iteration algorithm for Alzheimer's disease prediction," *Aging*, vol. 12, no. 7, pp. 6206–6224, Apr. 2020.

[51] Z. Zhou et al., "A toolbox for brain network construction and classification (BrainNetClass)," *Hum. Brain Mapping*, vol. 41, no. 10, pp. 2808–2826, Jul. 2020.

[52] R. Yu, Z. Han, A. Le, X. Chen, Z. Wei, and D. Shen, "Correlation-weighted sparse group representation for brain network construction in MCI classification," in *Medical Image Computing and Computer-Assisted Intervention—MICCAI*. Berlin, Germany: Springer, 2016.

[53] M. E. J. Newman, "Modularity and community structure in networks," *Proc. Nat. Acad. Sci. USA*, vol. 103, no. 23, pp. 8577–8582, Jun. 2006.

[54] J. Ma, J. Zhang, and Z. Wang, "Multimodality Alzheimer's disease analysis in deep Riemannian manifold," *Inf. Process. Manag.*, vol. 59, no. 4, Jul. 2022, Art. no. 102965.

[55] R. Hu et al., "Multi-band brain network analysis for functional neuroimaging biomarker identification," *IEEE Trans. Med. Imag.*, vol. 40, no. 12, pp. 3843–3855, Dec. 2021.

[56] Z. Wang et al., "Distribution-guided network thresholding for functional connectivity analysis in fMRI-based brain disorder identification," *IEEE J. Biomed. Health Informat.*, vol. 26, no. 4, pp. 1602–1613, Apr. 2022.

[57] Y. Zhang, H. Zhang, E. Adeli, X. Chen, M. Liu, and D. Shen, "Multiview feature learning with multiatlas-based functional connectivity networks for MCI diagnosis," *IEEE Trans. Cybern.*, vol. 52, no. 7, pp. 6822–6833, Jul. 2022.

[58] Y. Xue, Y. Zhang, L. Zhang, S.-W. Lee, L. Qiao, and D. Shen, "Learning brain functional networks with latent temporal dependency for MCI identification," *IEEE Trans. Biomed. Eng.*, vol. 69, no. 2, pp. 590–601, Feb. 2022.

[59] Z. Zhang, J. Ding, J. Xu, J. Tang, and F. Guo, "Multi-scale time-series kernel-based learning method for brain disease diagnosis," *IEEE J. Biomed. Health Informat.*, vol. 25, no. 1, pp. 209–217, Jan. 2021.

[60] K. Supekar, V. Menon, D. Rubin, M. Musen, and M. D. Greicius, "Network analysis of intrinsic functional brain connectivity in Alzheimer's disease," *PLoS Comput. Biol.*, vol. 4, no. 6, Jun. 2008, Art. no. e1000100.

[61] B. C. Dickerson et al., "Increased hippocampal activation in mild cognitive impairment compared to normal aging and AD," *Neurology*, vol. 65, no. 3, pp. 404–411, Aug. 2005.

[62] C. Hohenfeld, C. J. Werner, and K. Reetz, "Resting-state connectivity in neurodegenerative disorders: Is there potential for an imaging biomarker?" *NeuroImage, Clin.*, vol. 18, pp. 849–870, Jan. 2018.

[63] K. Mevel, G. Chételat, F. Eustache, and B. Desgranges, "The default mode network in healthy aging and Alzheimer's disease," *Int. J. Alzheimer's Disease*, vol. 2011, pp. 1–9, Jan. 2011.

[64] R. L. Buckner, J. R. Andrews-Hanna, and D. L. Schacter, "The Brain's default network: Anatomy, function, and relevance to disease," *Ann. New York Acad. Sci.*, vol. 1124, no. 1, pp. 1–38, Mar. 2008.

[65] L. Wang et al., "Changes in hippocampal connectivity in the early stages of Alzheimer's disease: Evidence from resting state fMRI," *NeuroImage*, vol. 31, no. 2, pp. 496–504, Jun. 2006.

[66] S. A. R. B. Rombouts, F. Barkhof, R. Goekoop, C. J. Stam, and P. Scheltens, "Altered resting state networks in mild cognitive impairment and mild Alzheimer's disease: An fMRI study," *Hum. Brain Mapping*, vol. 26, no. 4, pp. 231–239, Dec. 2005.

[67] M. L. Ries, T. W. Schmitz, T. N. Kawahara, B. M. Torgerson, M. A. Trivedi, and S. C. Johnson, "Task-dependent posterior cingulate activation in mild cognitive impairment," *NeuroImage*, vol. 29, no. 2, pp. 485–492, Jan. 2006.

[68] H. I. L. Jacobs et al., "Functional integration of parietal lobe activity in early Alzheimer disease," *Neurology*, vol. 78, no. 5, pp. 352–360, Jan. 2012.

[69] R. L. Buckner et al., "Molecular, structural, and functional characterization of Alzheimer's disease: Evidence for a relationship between default activity, amyloid, and memory," *J. Neurosci.*, vol. 25, no. 34, pp. 7709–7717, Aug. 2005.

[70] Y. Li et al., "Discriminant analysis of longitudinal cortical thickness changes in Alzheimer's disease using dynamic and network features," *Neurobiol. Aging*, vol. 33, no. 2, pp. 15–30, Feb. 2012.

[71] G. B. Frisoni, A. Prestia, P. E. Rasser, M. Bonetti, and P. M. Thompson, "In vivo mapping of incremental cortical atrophy from incipient to overt Alzheimer's disease," *J. Neurol.*, vol. 256, no. 6, pp. 916–924, Jun. 2009.

[72] H. Braak, I. Alafuzoff, T. Arzberger, H. Kretzschmar, and K. Del Tredici, "Staging of Alzheimer disease-associated neurofibrillary pathology using paraffin sections and immunocytochemistry," *Acta Neuropathologica*, vol. 112, no. 4, pp. 389–404, Oct. 2006.

[73] S. W. Scheff, D. A. Price, F. A. Schmitt, M. A. Scheff, and E. J. Mufson, "Synaptic loss in the inferior temporal gyrus in mild cognitive impairment and Alzheimer's disease," *J. Alzheimer's Disease*, vol. 24, no. 3, pp. 547–557, May 2011.